remote sensing

MDPI

Article

Quantifying the Effects of Normalisation of Airborne LiDAR Intensity on Coniferous Forest Leaf Area Index Estimations

Haotian You [1,2,†], Tiejun Wang [2,†], Andrew K. Skidmore [2] and Yanqiu Xing [1,*]

[1] Centre for Forest Operations and Environment, College of Engineering and Technology, Northeast Forestry University, Harbin 150040, China; wuliu2007_02@hotmail.com

[2] Faculty of Geo-Information Science and Earth Observation (ITC), University of Twente, P.O. Box 217, 7500 AE Enschede, The Netherlands; t.wang@utwente.nl (T.W.); a.k.skidmore@utwente.nl (A.K.S.)

* Correspondence: yanqiuxing@nefu.edu.cn; Tel.: +86-451-8219-1392

† These authors contributed equally to this work.

Academic Editors: Clement Atzberger and Prasad S. Thenkabail

Received: 9 December 2016; Accepted: 14 February 2017; Published: 16 February 2017

Abstract: The range between a sensor and the target, the incidence angle, and the target reflectance, are known factors that can influence the intensity values of LiDAR data and consequently, its use in many applications. However, very few studies have provided a quantitative analysis of the effects of normalisation of these three factors on forest leaf area index (LAI) estimations. In this paper, using two coniferous tree species (i.e., Scotch pine and Larch pine) as a case study, the effects of intensity normalisation on coniferous forest LAI estimations have, for the first time, been systematically examined and quantified. It was found that the intensity normalisation had a generally positive effect on the improvement of coniferous forest LAI estimations. However, the improvements were very minor. Specifically, the range normalisation did not improve the accuracy of the LAI estimation for either of the two coniferous tree species. The incidence angle and reflectance normalisation improved the accuracy of the LAI estimation for Scotch pine forests; however, they had no effect on the improvement of the LAI estimation for Larch pine forests. This experimental study suggests that range normalisation is not required for forest LAI estimations in areas with small elevation differences (i.e., less than 114 m). The incidence angle and target reflectance normalisation can marginally improve the accuracy of coniferous forest LAI estimations. However, the extent of this improvement varies among species, depending on the choice of incidence angle and reflectance coefficient. Overall, the effects of normalisation of airborne LiDAR intensity on coniferous forest LAI estimations are closely related to topographic conditions (i.e., elevation and slope), the tree species composition, and its associated structural attributes. Therefore, further research should explore the effects of LiDAR intensity normalisation on forest LAI estimations in regions with large elevation differences and diverse forest structures.

Keywords: range; incidence angle; target reflectance; laser penetration index; LAI

1. Introduction

Light Detection and Ranging (LiDAR) is an active optical remote-sensing technique that uses laser light to densely sample the Earth's surface. In addition to precise 3D coordinates, most LiDAR systems also record "intensity". The intensity value recorded by a LiDAR sensor, known as the reflection intensity, is equivalent to the amount of energy being emitted from a target. Most commercial LiDAR sensors have a wavelength in the near-infrared (NIR) spectral range. The LiDAR intensity data have been found to be directly related to the spectral reflectance of the reflected energy from objects in

the NIR wavelength [1]. As green vegetation strongly reflects energy in the NIR wavelength, LiDAR intensity data have been widely used for the mapping and monitoring of forest ecosystems [2–4].

The Leaf Area Index (LAI) is typically defined as the total one-sided area of green foliage per unit ground surface [5,6]. As a key canopy structural characteristic, and also a key component of biogeochemical cycles in ecosystems, the LAI serves as an important input or state variable for a variety of process-based ecological and biogeochemical models, such as forest growth estimations [7], fire behavior predictions [8] and ecological process modeling [9,10]. Airborne LiDAR pulses are able to penetrate forest canopies and even strike on the ground, thus allowing for a better characterization of all canopy layers [11], and at the same time, alleviating the saturation problem of traditional passive optical remote sensing for forests with a high LAI or biomass [12]. Consequently, a number of studies have recently been conducted with the aim of improving forest LAI estimations using airborne LiDAR intensity data. For example, Solberg [13] used the ratio variables based on the raw LiDAR intensity data to estimate the forest LAI and achieved a R^2 of 0.86. Peduzzi et al. [14] also used the raw mean intensity data and other variables to estimate the forest LAI and obtained a R^2 ranged from 0.71 to 0.83.

However, it is known that the intensity value recorded by the LiDAR sensor can be affected by the range between the sensor and the target, the incidence angle, the target surface reflectance, and the atmospheric transmission loss [15,16]. These factors can potentially increase the variability of intensity values and cause fine-scale speckling within the intensity imagery, making the interpretation difficult. The purpose of intensity normalisation is to remove the effect of the received energy with respect to the above mentioned factors. The research on the normalisation methods of LiDAR intensity has been an important topic in LiDAR applications in recent years [17–19]. The benefit of intensity normalisation has also been widely recognized [20–23]. For example, Mesas-Carrascosa et al. [24] discriminated the land uses by combining the normalised LiDAR intensity with digital images, and found that the classification accuracy can be over 92%. Yan et al. [25] studied the effects of intensity normalisation of LiDAR data on the land cover classification. They found that the accuracy could be improved by about 9.4%–12.8%, after the geometric calibration and radiometric correction of intensity data. Korpela et al. [26] compared the performance of the raw intensity data and range-normalised intensity data for tree species classification. They found that the range-normalised intensity data could improve the classification accuracy by 2%–3%. Hofle et al. [27] also indicated that when the LiDAR data is acquired in mountainous areas with large elevation differences, the uncorrected intensity values and images cannot be used directly. This implies that, if the intensity data are to be used for the retrieval of higher level products such as LAI and subsequently, in different applications, a proper radiometric normalisation is essential [28].

Many efforts on the radiometric normalisation of LiDAR intensity data have been carried out to improve the accuracy of forest LAI estimations. For example, Hopkinson and Chasmer [29] used the square root power ratio to correct the intensity power ratio, accounting for the transmission losses both in and out of the forest canopy, and consequently, to estimate the forest LAI and gap fraction. They found that it performed well across a range of forest types. Heiskanen et al. [30] used the range to normalise the raw intensity and found that the intensity cover index provided the best model fit for the forest LAI, when all plots were pooled. They concluded that the estimation results were satisfactory. However, whether the range normalisation could improve the accuracy of estimating the LAI was not categorically demonstrated in their studies. Solberg [31] used the reflectance ratio between the ground and canopy to correct the intensity-based laser penetration index (LPI), and found that the most accurate estimation could be achieved when the ratio was set at five, rather than at one. Luo et al. [32] used the intensity data normalised by the range, incidence angle, and a fixed reflectance coefficient to estimate the forest LAI, and achieved better results than when using raw intensity data. They concluded that intensity normalisation could improve the estimation accuracy. However, all of these studies did not provide any specific advice on which factor should be normalised in a specific circumstance, when the intensity was applied to forest LAI estimations. To maximise the cost savings and improve computational efficiency, it is necessary to systematically study and quantify the effects

of normalisation of airborne LiDAR intensity data by different factors, when estimating the forest LAI. As one of the most productive forests, the coniferous forest LAI has been studied using airborne LiDAR data [33,34]. However, the study on the difference of forest LAI estimations between different coniferous tree species has seldom been reported.

This study aims to use different factors, including the range between LiDAR sensor and targets, the incidence angle, and the target reflectance, to normalise the airborne LiDAR intensity data. Then, the laser penetration index (LPI) extracted from raw and normalised intensity data is used to estimate the forest LAI, based on the Beer-Lambert law [33]. In the final assessment process, two different coniferous tree species are used to systematically quantify the effects of intensity normalisation on forest LAI estimations.

2. Materials and Methods

2.1. Study Area

The study area is located in the Moon Lake National Forest Park, China (WGS84 43°46′N, 125°27′E) (Figure 1), and it covers an area of about 2500 hectares with an elevation ranging from about 220 to 406 m. The study area is dominated by two coniferous tree species: Scotch pine (*Pinus sylvestris* L.) and Larch pine (*Larix cajanderi*), with small amounts of Mongolian oak (*Quercus mongolica*), aspen (*Populus davidiana*), and other tree species. The Scotch pine is characterised by open crowns with long needle-like leaves in bundles of two, from 4 to 9 cm (Figure 2a), with an irregular, domed and flat crown, although some young trees are slightly conical near their tops. The Larch pine is characterised by an open, narrow conic crown with needle-like leaves clustered on branches, which are shorter than those of the Scotch pine trees, ranging from 1.5 to 3 cm (Figure 2b).

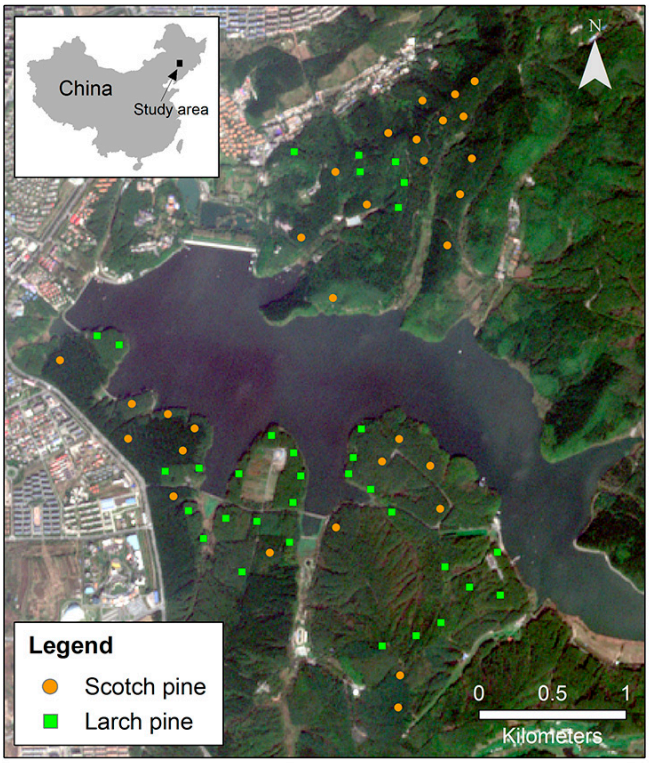

Figure 1. Location of the study area in China, and the distribution of sample plots on a natural color composite of Sentinel-2A image acquired in October 2016.

(**a**) (**b**)

Figure 2. Graphic representation: (**a**) Scotch pine; (**b**) Larch pine.

2.2. In-Situ Measurements of Forest LAI

Fieldwork was carried out in July 2014 using a stratified random sampling strategy. Forest type maps were obtained from the Moon Lake National Forest Park. Based on the forest types, the study area was stratified into Scotch pine-dominated and Larch pine-dominated areas. A total of 80 plots were randomly selected over the two forest types. In the field, 17 plots were found to be mixed with other tree species and were removed from the survey. As a result, only 63 plots with pure species were measured, including 30 Scotch pine plots and 33 Larch pine plots. The forests in these plots are dense, mature (more than 50 years), and unmanaged. The ground cover was dominated by bare soil and litter. Information on the tree density, tree height, elevation, and slope within these plots, are shown in Table 1. The radius of each plot was 10 m, and a Trimble GeoXH 6000 GPS, in combination with a South Total Station NTS 312B, were used to record the center location of each plot (with an accuracy of approximately 2 m).

Table 1. Descriptive statistics of the field sample plots (plot number = 63).

Tree Species	Variable	Mean	Minimum	Maximum
Scotch pine	LAI	2.56	2.03	3.61
	Tree density (trees/ha)	900	500	1900
	Tree height (m)	16.0	12.1	19.7
	Elevation (m)	293	244	358
	Slope (degree)	9	1	30
Larch pine	LAI	2.86	2.54	3.32
	Tree density (trees/ha)	1200	800	2200
	Tree height (m)	19.0	14.3	24.4
	Elevation (m)	266	250	304
	Slope (degree)	8	1	18

The in-situ canopy LAI was collected using digital hemispherical photography, which is regarded as the best ground-based technique for measuring the LAI [35–38]. The digital hemispherical photographs (Figure 3) were taken using a Samsung NV3 camera with a fish-eye lens, placed at a height of 1.5 m above the ground level and facing true north. Within each plot, five hemispherical photographs were separately acquired from the centre, and from 5 m in each cardinal direction. In addition, all of the hemispherical photographs were collected under diffuse lighting conditions, to avoid the effect of direct sunlight on the LAI estimation.

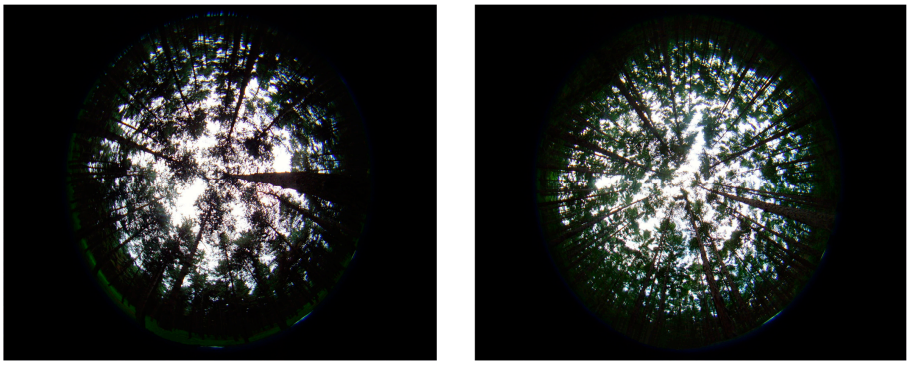

(**a**) (**b**)

Figure 3. Examples of collected digital hemispherical photographs for: (**a**) Scotch pine; (**b**) Larch pine.

The digital hemispherical photographs were analysed using WinSCANOPY 2010 (Regent Instruments, Québec, QC, Canada) software. It computed the forest LAI based on the classification of pixels as either white (sky) or black (canopy). Since the method does not distinguish the sky obstructed by leaves, branches, and stems, and does not correct the clumping effect, the LAI calculated with this method is called effective LAI. The effective LAI does not affect the quality of the LAI estimation model [9], and the difference between an effective LAI and a true LAI, is a proportional coefficient, which is about 1.75 [39]. Therefore, the effective LAI, instead of true LAI, is used in this paper. Descriptive statistics of the in-situ canopy LAI are presented in Table 1.

2.3. LiDAR Data and Pre-Processing

The airborne LiDAR data were acquired on 31 May 2012, using a Leica ALS70 LiDAR sensor carried by a helicopter. The wavelength was 1064 nm and the scan angle range was $\pm 20^{\circ}$. The nominal flying altitude was approximately 560 m above the ground level. The point clouds covering the study area were generated from seven swaths. There was about a 40% overlap between two adjacent swaths.

The acquired LiDAR data containing the coordinates and intensity information were pre-processed to eliminate the noise points. At the same time, the swaths overlap point clouds were also cut off, to eliminate the effect of overlap on the forest LAI estimation. As a result, the mean density of the LiDAR points is about nine points per m^2. The pre-processed points were classified into ground points and non-ground points, by using the filter algorithm of the triangulated irregular network. Then, the ground points were used to generate the digital elevation model (DEM) with the triangulated irregular network interpolation algorithm [40,41]. All of the above operations were achieved with Terrasolid software (Terrasolid Ltd., Hesinki, Finland). Subtracting the corresponding elevation of the DEM generated the height above the ground surface for every non-ground point. The points above 1.5 m were classified as vegetation points. All of the pre-processed points, except for the vegetation points, were considered as ground points. The height threshold of 1.5 m coincided with the height of the fisheye lens when the hemispherical photographs were taken, which was proven as the best choice for the forest LAI estimation in the research of Sumnall et al. [42].

2.4. LiDAR Intensity Data Normalisation

The airborne LiDAR system works under the same physical principle as a radar and follows the radar equation [43], presented in Equation (1). The intensity recorded by the LiDAR system is affected by the LiDAR sensor configuration, object characteristics, and atmospheric parameter. The sensor configuration parameters include: the transmitted pulse power P_t, the sensor aperture size D_r, the range between the sensor and target R, the beam (pulse) divergence β_t, and the system gain η_{sys}. The object characteristic refers to the backscatter cross-section σ. The atmospheric parameter refers to the atmospheric attenuation η_{atm}. The received pulse intensity P_r can be defined as follows:

$$P_r = \frac{P_t D_r^2}{4\pi R^4 \beta_t^2} \eta_{sys} \eta_{atm} \sigma \tag{1}$$

Under a series of assumptions and equivalent transformations [27,44], the σ could be expressed as a function of target reflectance ϱ, the range between the sensor and target R, the beam (pulse) divergence β_t, and the incidence angle α, as presented in Equation (2) [43].

$$\sigma = \pi \rho R^2 \beta_t^2 \cos\alpha \tag{2}$$

In a single flight campaign, some specific parameters, such as P_t, D_r, η_{sys}, and η_{atm}, are supposed to be same, and could be regarded as constant values [45,46]. Based on this assumption and simplification, Equation (1) can be reformed as Equation (3):

$$P_r = \frac{\rho}{R^2} \times \cos\alpha \times C \tag{3}$$

where C is a constant standing for P_t, D_r, η_{sys}, and η_{atm}.

2.4.1. Range Normalisation

During the range normalisation of the intensity data, the target reflectance and incidence angle are both regarded as constant, which is the most widely used method [47,48]. The normalised intensity is defined as:

$$I_R = I_{original} \times \frac{R^2}{R_{ref}^2} \tag{4}$$

$$R = \frac{R_{ref} - R'}{\cos\theta} \tag{5}$$

where I_R and $I_{original}$ are the range-normalised and original intensity data, respectively, R is the actual range between the sensor and the target, R_{ref} is the reference distance, R' is the elevation of echo, and θ is the scan angle.

2.4.2. Incidence Angle Normalisation

The incidence angle is defined as the angle between the normal target surface and the direction of the incident laser pulse, which is influenced by the topography of the target surface, scan angle, and flight line [49]. Its calculation equation is presented in Equation (6), whose detailed derivation procedure can be found in the paper of Yan and Shaker [46].

$$\alpha = \cos^{-1}[\cos\theta\cos\varphi + \sin\theta\sin\varphi\cos(\beta - \theta_h)] \tag{6}$$

where φ is the slope, β is the aspect, and θ_h is the projected horizontal angle.

Under the assumption of Lambertian scattering characteristics, the reflected intensity is proportional to cos(α) [50]. Therefore, the incidence angle normalisation method defined in Equation (7) is selected.

$$I_\alpha = I_{original} \times \frac{\cos\left(\alpha_{ref}\right)}{\cos(\alpha)} \tag{7}$$

where I_α is the incidence angle normalised intensity data and α_{ref} is the standard incidence angle ($\alpha = 0^\circ$) [51].

2.4.3. Target Reflectance Normalisation

The target reflectance is another important parameter affecting the intensity and its theoretical normalisation is shown in Equation (8).

$$I_\rho = I_{original} \times \frac{\rho_{ref}}{\rho} \tag{8}$$

where I_ρ is the target reflectance-normalised intensity data, ρ is the target reflectance, and α_{ref} is the reference reflectance.

It is difficult to obtain the true surface reflectance of different natural objects for the majority of research studies. Therefore, the reflectance coefficient (K_S) is introduced as a proxy and is used to eliminate the intensity difference between two different surfaces [31]. As determined from the field investigation, the ground cover and the surface of each coniferous tree species are considered to be homogeneous. Therefore, the surface reflectance of the forest area could be simplified to three kinds of reflectance values, individually representing the Scotch pine forest canopy surface (ρ_S), the Larch pine forest canopy surface (ρ_L), and the ground surface (ρ_G). Two K_S values are calculated from the above three surface reflectances, presented in Equations (9) and (10) [9,52].

$$K_S = \frac{\rho_G}{\rho_S} \tag{9}$$

$$K_L = \frac{\rho_G}{\rho_L} \tag{10}$$

where K_S is the reflectance coefficient of the Scotch pine canopy surface and ground surface, K_L is the reflectance coefficient of the Larch pine canopy surface and ground surface, ρ_S is the reflectance of the Scotch pine canopy surface, ρ_L is the reflectance of the Larch pine canopy surface, and ρ_G is the reflectance of the ground surface.

2.5. Laser Penetration Index Extraction

By taking the transmission of the laser beams through the canopy into account, the laser penetration index (LPI) is the most commonly used variable for forest LAI and gap fraction estimations [33,53,54]. Therefore, the LPI was selected and computed, based on the raw and normalised LiDAR intensity data within each plot (Table 2). The detailed computational procedures of LPI are described in Equations (11)–(13).

$$LPI = \frac{\sum I_G}{\sum I_G + \sum I_V} \tag{11}$$

$$LPI = \frac{\sum I_{GNormalised}}{\sum I_{GNormalised} + \sum I_{VNormalised}} \tag{12}$$

$$LPI = \frac{\sum I_{GNormalised}}{\sum I_{GNormalised} + \sum I_{VNormalised}} = \frac{{\rho_G}^{-1} \times \sum I_G}{{\rho_G}^{-1} \times \sum I_G + {\rho_V}^{-1} \times \sum I_V} = \frac{\sum I_G}{\sum I_G + K \times \sum I_V} \tag{13}$$

where $\sum I_G$ is the sum of the original intensity of ground points, $\sum I_{GNormalised}$ is the sum of the normalised intensity of ground points, $\sum I_V$ is the sum of the original intensity of vegetation points, $\sum I_{VNormalised}$ is the sum of the normalised intensity of vegetation points, ρ_V is the reflectance of the vegetation surface, and K is the reflectance coefficient of the ground surface and the vegetation surface.

Table 2. Description of the LiDAR intensity variables.

Variables	Description
LPI	LPI extracted from the original intensity data
LPI_R	LPI extracted from the range-normalised intensity data
LPI_A	LPI extracted from the incidence angle-normalised intensity data
LPI_K	LPI extracted from the reflectance coefficient-normalised intensity data

2.6. Forest LAI Estimation and Accuracy Assessment

To estimate the forest LAI, the Beer-Lambert law, based on forest gap fraction, presented in Equation (14), was used, which is the most common algorithm used by field LAI measurement instruments and airborne LiDAR point cloud data [31,32].

$$LAI = -\beta \ln(LPI) \tag{14}$$

where β is the fitting coefficient.

To assess the predictive ability of the model, it is advised that sufficient validation field data are provided, which are different from the model training data. However, there are limited field data in this study. In order to avoid the influence of random factors and obtain reliable estimation results with limited plots, the leave-one-out-cross-validation method (LOOCV) was applied in this paper [55]. The coefficient of determination (R^2) and the root mean square error (RMSE) were used as the estimators of model accuracy.

3. Results

3.1. Range Normalisation

For Scotch pine forests, the relationship between the field-measured and LiDAR-predicted LAI, based on the raw intensity data (i.e., LPI) and range-normalised intensity data (i.e., LPI_R), is presented in Figure 4. It shows that, without range normalisation, the Scotch pine forest LAI was estimated with a R^2 of 0.794 and a RMSE of 0.172 (Figure 4a). After range normalisation, R^2 slightly improved to 0.795 and RMSE remained unchanged (Figure 4b). This means that the range normalisation of LiDAR intensity data, only very marginally improved the accuracy of the LAI estimation for Scotch pine forests.

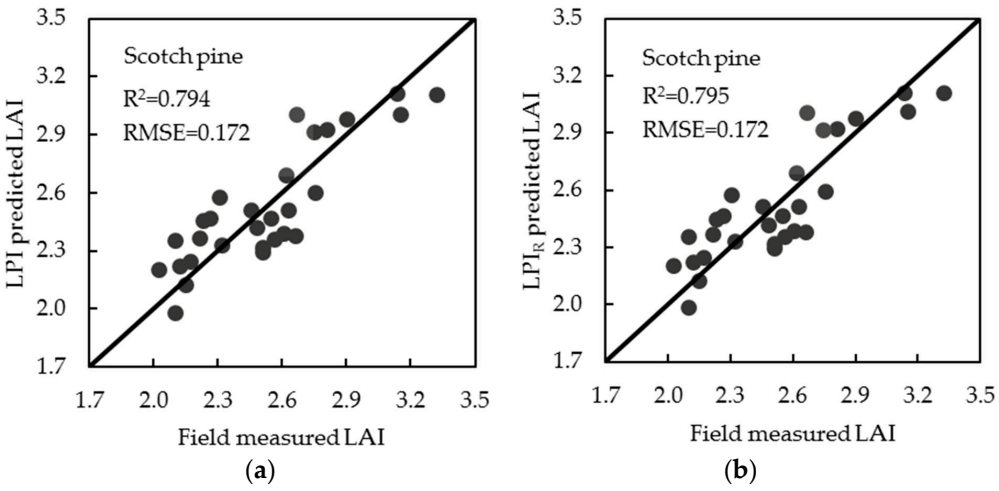

Figure 4. The 1:1 relationship between the field-measured LAI and LiDAR-predicted LAI for Scotch pine forests based on: (**a**) the raw intensity data (i.e., LPI); (**b**) the range-normalised intensity data (i.e., LPI_R). R^2 and RMSE are values from leave-one-out cross-validation.

For Larch pine forests, the relationship between the field-measured and LiDAR-predicted LAI, based on the raw intensity data (i.e., LPI) and the range-normalised intensity data (i.e., LPI_R), is presented in Figure 5. It shows that, before and after range normalisation, the Larch pine forest LAI was estimated with the same accuracy, which obtained a R^2 of 0.762 and a RMSE of 0.091 (Figure 5a,b). This means that the range normalisation of LiDAR intensity data failed to improve the accuracy of the LAI estimation for Larch pine forests.

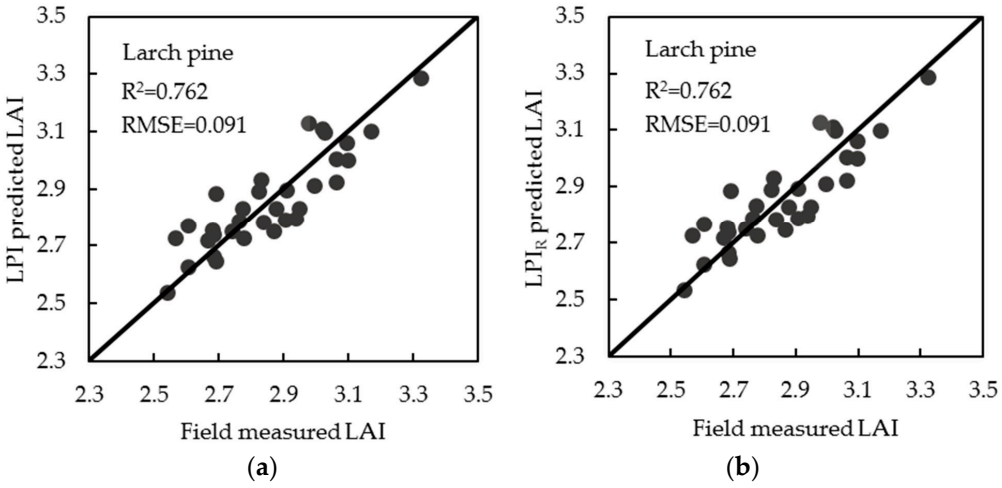

Figure 5. The 1:1 relationship between the field-measured LAI and LiDAR-predicted LAI for Larch pine forests based on: (**a**) the raw intensity data (i.e., LPI); (**b**) the range-normalised intensity data (i.e., LPI_R). R^2 and RMSE are values from leave-one-out cross-validation.

3.2. Incidence Angle Normalisation

To avoid the overcorrection of intensity values, different incidence angles, such as 0°, 5°, 10°... 70° and 75°, were applied to correct the LiDAR intensity data from the forest canopy, for both Scotch pine and Larch pine forests. The LAI estimation results for the Scotch pine forest with different incidence angles, are presented in Figure 6. They show that the highest estimation accuracy was achieved with a R^2 of 0.806 and a RMSE of 0.167, when the incidence angle threshold was set to 55° (Figure 6a). The relationship between the field-measured LAI and LiDAR-predicted LAI with the optimal incidence angle (i.e., $LPI_{A=55°}$), is presented in Figure 6b. By comparing the LAI estimation results shown in Figure 4a (without incidence angle normalisation) and Figure 6b (with incidence angle normalisation), it was found that the LAI estimation for Scotch pine forests was improved after the incidence angle normalisation, with an increase in the R^2 of 0.012 and a decrease in the RMSE of 0.005. This result suggests that incidence angle normalisation can improve the LAI estimation for Scotch pine forests, but that this improvement is only marginal.

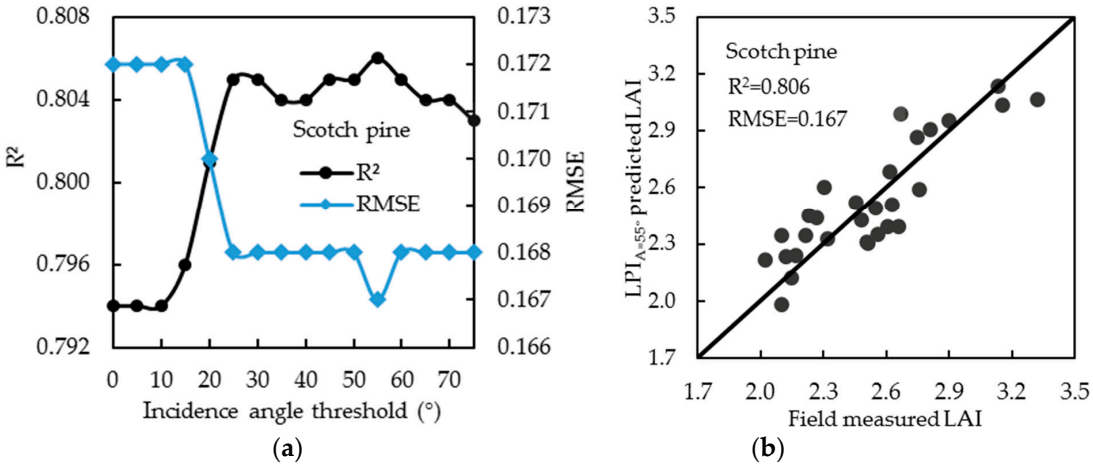

Figure 6. The LAI estimation results for Scotch pine forests with incidence angle normalisation: (**a**) LAI estimation accuracy with different incidence angles; (**b**) The relationship between the field-measured LAI and LiDAR-predicted LAI when incidence angle threshold was set to 55° (i.e., $LPI_{A=55°}$). R^2 and RMSE are values from leave-one-out cross-validation.

The LAI estimation results for Larch pine forests with different incidence angles are presented in Figure 7. It also shows that the highest estimation accuracy was achieved with a R^2 of 0.763 and a RMSE of 0.091, when the incidence angle threshold was set to 55°. The relationship between the field-measured LAI and LiDAR-predicted LAI with the optimal incidence angle (i.e., $LPI_{A=55°}$), is presented in Figure 7b. By comparing the results shown in Figure 5a (without incidence angle normalisation) and Figure 7b (with incidence angle normalisation), it was found that the LAI estimation for Larch pine forests was very marginally improved after incidence angle normalisation, with a minor increase in the R^2 of 0.001 and an unchanged RMSE. This result suggests that incidence angle normalisation cannot improve the LAI estimation for Larch pine forests.

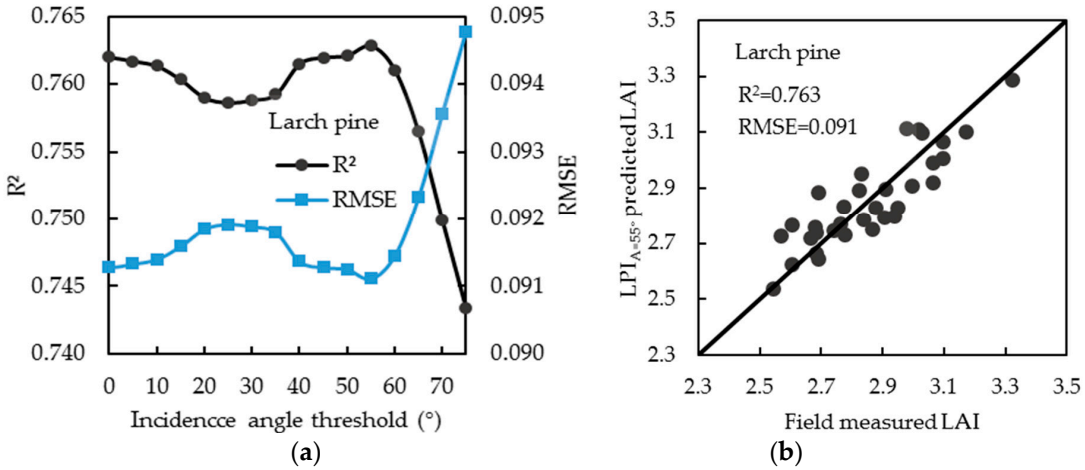

Figure 7. The LAI estimation results for Larch pine forests with incidence angle normalisation: (**a**) LAI estimation accuracy with different incidence angles; (**b**) The relationship between the field-measured LAI and LiDAR-predicted LAI when incidence angle threshold was set to 55° (i.e., $LPI_{A=55°}$). R^2 and RMSE are values from leave-one-out cross-validation.

3.3. Target Reflectance Normalisation

To obtain the optimal LAI estimation results for Scotch pine and Larch pine forests under reflectance coefficient normalisation, different K values of 0.1, 0.5, 1.0, 1.5, 2.0... 5.5, 6.0, and 7.0, were used, respectively. The LAI estimation results for Scotch pine forests with different K values are presented in Figure 8. It shows that the highest estimation accuracy was achieved with a R^2 of 0.810 and a RMSE of 0.166, when the K value was set to around 0.1, with the R^2 showing a declining trend as the K increased up to a value of 6 (Figure 8a). The relationship between the field-measured LAI and LiDAR-predicted LAI with the optimal K value of 0.1 (i.e., $LPI_K = 0.1$), is presented in Figure 8b. By comparing the results shown in Figure 4a (without target reflectance normalisation) and Figure 8b (with target reflectance normalisation), it was found that the LAI estimation for Scotch pine forests improved after target reflectance normalisation, with an increase in the R^2 of 0.016 and a decrease in the RMSE of 0.006. This result suggests that target reflectance normalisation can improve the LAI estimation for Scotch pine forests, but that this improvement is only minor.

The LAI estimation results for Larch pine forests with different K values are presented in Figure 9. It shows that the highest estimation accuracy was achieved with a R^2 of 0.762 and a RMSE of 0.091, when the K value was set to around 1, with the R^2 showing an increasing trend up to 1, and then a declining trend until it became stable (Figure 9a). The relationship between the field-measured LAI and LiDAR-predicted LAI with the optimal K value (i.e., $LPI_{K=1}$), is presented in Figure 9b. By comparing the results shown in Figure 5a (without target reflectance normalisation) and Figure 9b (with target reflectance normalisation), it was found that the LAI estimation for Larch pine forests

remains unchanged after target reflectance normalisation. This result suggests that target reflectance normalisation cannot improve the LAI estimation for Larch pine forests.

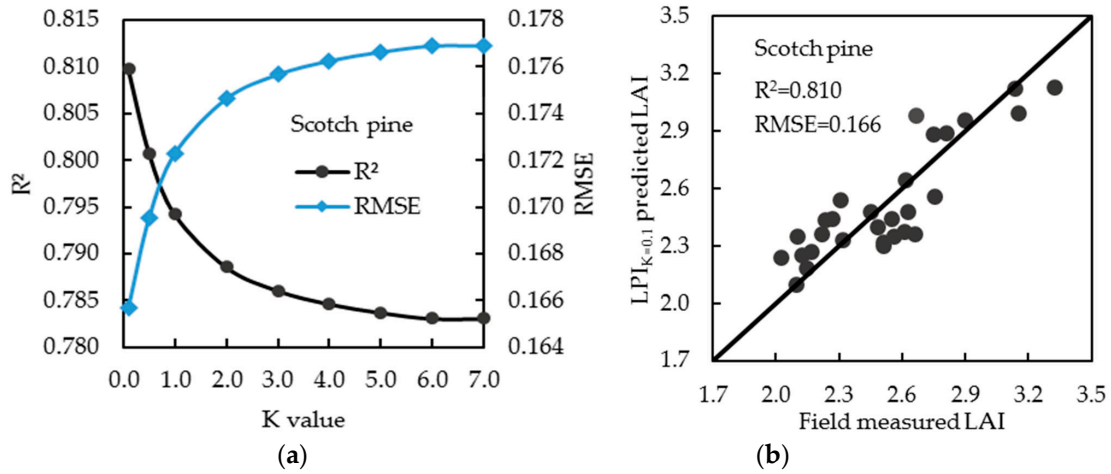

Figure 8. The LAI estimation results for Scotch pine forests with target reflectance normalisation: (**a**) LAI estimation accuracy with different K values; (**b**) The relationship between the field-measured LAI and LiDAR-predicted LAI when the K value was set to around 0.1 (i.e., $LPI_{K=0.1}$). R^2 and RMSE are values from leave-one-out cross-validation.

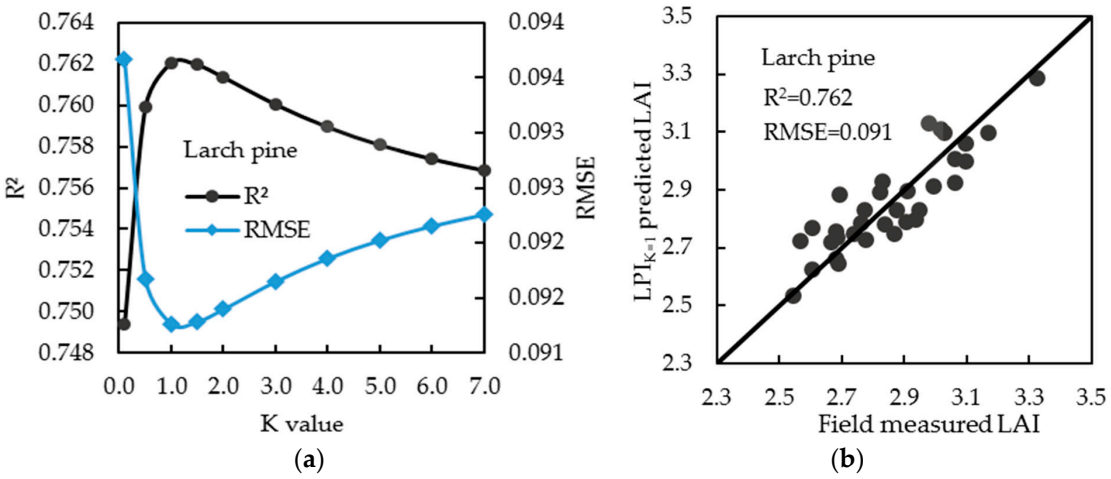

Figure 9. The LAI estimation results for Larch pine forests with target reflectance normalisation: (**a**) LAI estimation accuracy with different K values; (**b**) The relationship between the field-measured LAI and LiDAR-predicted LAI when the K value was set to around 1 (i.e., $LPI_{K=1}$). R^2 and RMSE are values from leave-one-out cross-validation.

4. Discussion

4.1. Effect of Range Normalisation on Forest LAI Estimation

Previous studies suggest that variation in LiDAR intensity data, caused by the range differences between the sensor and target, is the most important factor, which should be accounted for by range normalisation in various applications [21,56]. This is because range normalisation could project the original intensity onto a reference range, removing the path length variations and range dependence of the intensity. The benefit of range-normalised data has been confirmed by land cover classification studies. Although some researchers have used range-normalised intensity data to estimate the forest LAI [29,30,57], the difference between the pre- and post-normalised intensity on forest LAI estimations

has never been reported. In this paper, we observed that the range normalisation of LiDAR intensity data made very minor, or no improvements, on the LAI estimation accuracy of a coniferous forest. These findings are different from the results reported in previous land cover classification studies. For example, Gatziolis [48] studied the effect of range normalisation of LiDAR intensity data on the vegetation type classification. It was found that the accuracy from range-normalised intensity data was 28.9% higher than the result from the raw intensity data. The contrasting results may be explained by three reasons. Firstly, most research on land cover classification is based on the use of one class of normalised LiDAR intensity data, such as the ground points class or vegetation points class. However, for forest LAI estimations, the laser penetration index (LPI) calculated from the airborne LiDAR intensity data is a ratio variable, which uses both the ground points class and vegetation points class. The ratio of the two points classes may mitigate the effect of range normalisation of the LiDAR intensity data, because the LPI extracted from the normalised intensity data is not only related to the intensity sum of ground points, but also to the intensity sum of vegetation points. In essence, it is not related to the plot elevation, but to the tree height. Secondly, the small elevation difference may be another reason why results demonstrate little effect of range normalisation on forest LAI estimations. In our study area, the elevation difference between field plots was relatively small, with a maximum difference of about 114 m. Although the mean tree height of Larch pine forests is higher than the mean tree height of Scotch pine forests (as shown in Table 1), the difference in the mean tree height is only ~3 m and seems relatively small, compared with the difference in plot elevation. Therefore, the elevation difference still plays a major role in range intensity normalisation. Lastly, it may be because of the use of different laser return echoes. This is in agreement with Gatziolis [48], who observed that the vegetation type classification accuracy from the range-normalised intensity of single returns was 20% higher than the accuracy from the range-normalised intensity of first and single returns. In view of this, different laser return echoes should be studied separately, in order to understand the effect of range normalisation of different laser return echoes on forest applications.

The results of this study also demonstrated that there was no significant difference on the effects of range normalisation between Scotch pine and Larch pine forests. This was caused by the small elevation differences between Scotch pine and Larch pine plots. As shown in Table 1, the maximum elevation difference of Scotch pine plots was 114 m, while the elevation difference of Larch pine plots was 79 m. A difference of only 35 m might not influence the model's performance. Although the elevation range in our study area was relatively small, it still stands for an important topography class for forest resources distribution, including plain, low mountains, and hills. Therefore, the results derived from the current study could provide advice for forest applications in these areas. When the LPI variable is used to estimate the forest LAI, it is not necessary to normalise the intensity data with the range, if the elevation difference is less than 114 m. Therefore, whether there is a need for range normalisation should be decided, based on the variable used and the topographic conditions of the study area.

4.2. Effect of Incidence Angle Normalisation on Forest LAI Estimation

For incidence angle normalisation, it was observed that an intensity overcorrection occurs when the incidence angle was directly applied to normalise the LiDAR intensity data from the forest canopy [25,27,51]. This is mainly because the majority of incidence angles derived from the digital surface model were achieved at 90°. The incidence angle normalisation did not follow the radar equation when the incidence angle was more than a threshold angle. Therefore, the selection of the threshold angle was critical for the incidence angle normalisation of LiDAR intensity from the forest surface. At the same time, our results also proved that the use of an optimal incidence angle threshold value could avoid the overcorrection of LiDAR intensity data and improve the accuracy of forest LAI estimation. A similar conclusion was also reported by Yan and Shaker [45]. They corrected the LiDAR intensity data with a slope threshold and then used the corrected intensity to classify the land cover. They found that the coefficient of variation of the land cover samples became larger after the incidence

angle exceeded one slope threshold (30–40°). This marginal improvement could be explained by the following reasons. The slope and aspect used for calculating the incidence angle are not the real surface-reflected echo pulses. This would make the intensity normalisation inappropriate and limit further improvement of the accuracy of forest LAI estimations. Furthermore, the incidence angle normalisation is based on the radar equation, which assumes that all targets are ideal Lambertian scatters. However, the forest does not satisfy this assumption, which also limits the improvement of the estimation accuracy to some extent. Therefore, the introduction of a new and more suitable method is of importance for future research on incidence angle intensity normalisation.

The incidence angle has an effect on LiDAR intensity data [27,49]. However, the effect of incidence angle intensity normalisation is dependent on the choice of the incidence angle and the forest structure. As the previous research concluded, when the scan angle was less than 15°, the effect of the scan angle could be neglected [9,15,58]. In this study, incidence angle intensity normalisation had an effect on the LAI estimation for Scotch pine forests, but had little, or no effect, on the LAI estimation for Larch pine forests. It demonstrated that the incidence angle derived from the digital surface model had an effect on the intensity, and that this effect was closely related to the forest structure. When the forest surface was flatter, incidence angle intensity normalisation had a greater effect on improving the accuracy of forest LAI estimations. When the forest surface was steeper, the effect was small. Therefore, in the future, the need for incidence angle intensity normalisation should be dependent on the choice of the incidence angle and the forest structure. Additionally, the results also demonstrated that the incidence angle threshold method may be a good choice for forest intensity normalisation.

4.3. Effect of Target Reflectance Normalisation on Forest LAI Estimation

The most accurate forest LAI estimation results appeared when different reflectance coefficients were used for the two coniferous tree species. For the Scotch pine forest, the estimation accuracy reached a peak when the K value was set to 0.1. For the Larch pine forest, the model performs with the highest accuracy when the K value was set to 1. This K value is smaller than the one derived from the research of Solberg [30], who also estimated the LAI for Scotch pine forests using the LPI from normalised LiDAR intensity with K. They found that the result reached a peak when the K value was set to 5. Generally, the K value varies, due to the differences between the ground and forest canopy reflectance. In the study of Solberg [30], the ground was reported to be covered with lichens, whilst in our study area, the ground is dominated by bare soil and litter. The forest canopy reflectance data used by Solberg [30] were acquired during a severe pine sawfly attack, while the data used in this paper were acquired under normal circumstances (i.e., healthy forest). Meanwhile, the Scotch pine forest consisted of young, intermediate, and old age classes in the research of Solberg [30], while only one mature age class of forests was used in this paper. Furthermore, all of the crown densities used in this paper were above 80%, which potentially had a significant influence on the canopy reflectance [59].

For Scotch pine and Larch pine forests, the K values were different. This difference indicated that the 1064 nm wavelength had a higher separability for the spectral reflectance, which could be used to discriminate the difference between different coniferous tree species. Since the true reflectance of different targets was not available in this study, the difference of reflectance coefficients could only be analysed from both the forest ground composition and the canopy structure. The ground layer of this study area consisted of bare soil and litter. Therefore, there is almost no significant difference between the Scotch pine and Larch pine plots, both with a mean ground intensity value of about 102 W. The reason for this is most likely explained by the difference in the canopy structure of the two different tree species. For the Scotch pine forest, when the tree is mature, the crown is flat with longer needle leaves, from 4 to 9 cm. For the Larch pine forest, the crown is ovate-conical, with more, short needle-like leaves clustered on branches, from 1.5 to 3 cm. Therefore, the fraction of the LiDAR footprint blocked by the Scotch pine needle leaves is relatively high, reducing the loss of intensity. Relatively speaking, the fraction of the footprint which is blocked by Larch pine short needle-like leaves is smaller, enhancing the loss of intensity. The structural difference makes the intensity of the

Scotch pine canopy higher, when compared to the intensity of the Larch pine forest canopy. For the Scotch pine forest, the average intensity value of the vegetation was approximately 133 W, which is about 46 W higher than the intensity value of the Larch pine forests.

Obtaining the target reflectance still remains a problem for LiDAR intensity normalisation, although it was proven to be important in normalising the intensity [13]. In this case, an alternative way of obtaining the reflectance coefficient was used, and it was proven that different tree species had different reflectance coefficients. Therefore, before the reflectance coefficient can be used, it must be carefully examined and the best one for each tree species should be selected. In the future, if the target's true reflectance could be easily obtained, then the reflectance-normalised intensity data should be more accurate and widely used in forest applications.

From the above results, it was found that for the Scotch pine forest LAI estimation, intensity normalisation of the incident angle and target reflectance could improve the estimation accuracy, while intensity normalisation of the range showed a very minor effect on the improvement of the forest LAI estimation. For the Larch pine forest LAI estimation, all of the effects of intensity normalisation with the range, incidence angle, and target reflectance, were so small that they could be neglected. Therefore, the factor which should be normalised first should be determined based on the specific circumstances, for example, the topographic conditions of the study area, the forest structure, the tree species composition, and the nature of the metrics. When it is not known which factor should be normalised, the comprehensive normalisation of all available factors may be a good choice, except for reducing the computational efficiency and not improving the accuracy to the maximum extent. When the effect of each factor is known, the targeted normalisation may be the best choice for improving the estimation accuracy.

5. Conclusions

In this paper, three different factors, including the range, incidence angle, and target reflectance, were applied independently, to normalise the LiDAR intensity data. Subsequently, the laser penetration indices (LPI) derived from the raw and normalised intensity data were used to estimate the forest LAI, based on the Beer-Lambert law. Finally, two coniferous tree species were tested to systematically examine and quantify the effects of intensity normalisation on coniferous forest LAI estimations. The main conclusions that can be drawn from the present study are:

(1) Generally, intensity normalisation has a positive effect on the improvement of LAI estimations in coniferous forests. However, this improvement is very minor.
(2) The range normalisation cannot improve the accuracy of the coniferous forest LAI estimation, when the LPI is applied in areas with small elevation differences.
(3) The incidence angle and target reflectance normalisation could improve the accuracy of coniferous forest LAI estimations. However, the extent of this improvement varies among species, depending on the choice of incidence angle and reflectance coefficient.

Overall, the effects of normalisation of airborne LiDAR intensity on coniferous forest LAI estimations are closely related to the topographic conditions (i.e., elevation and slope), tree species composition, and its associated structural attributes. Therefore, further research should explore the effects of LiDAR intensity normalisation on forest LAI estimations in regions with large elevation differences and diverse forest structures.

Acknowledgments: This work is supported by the Fundamental Research Funds for the Central Universities (No. 2572015AB15) and the Special Fund for Forest Scientific Research in the Public Welfare (No. 201504319).

Author Contributions: Haotian You, Yanqiu Xing, Tiejun Wang and Andrew Skidmore conceived and designed the experiments; Haotian You and Yanqiu Xing performed the experiments; Haotian You and Tiejun Wang analysed the data and wrote the paper; all authors contributed to the editing of the manuscript.

Conflicts of Interest: The authors declare no conflict of interest. The founding sponsors had no role in the design of the study; in the collection, analyses, or interpretation of data; in the writing of the manuscript, and in the decision to publish the results.

References

1. Shaker, A.; Yan, W.Y.; El-Ashmawy, N. The effects of laser reflection angle on radiometric correction of airborne LiDAR intensity data. *Int. Arch. Photogramm. Remote Sens. Spat. Inf. Sci.* **2011**, *3812*, 213–217. [CrossRef]
2. Dubayah, R.O.; Drake, J.B. Lidar remote sensing for forestry. *J. For.* **2000**, *98*, 44–46.
3. Maltamo, M.; Næsset, E.; Vauhkonen, J. *Forestry Applications of Airborne Laser Scanning: Concepts and Case Studies*; Springer: Dordrecht, The Netherlands, 2014.
4. Hovi, A.; Korhonen, L.; Vauhkonen, J.; Korpela, I. Lidar waveform features for tree species classification and their sensitivity to tree-and acquisition related parameters. *Remote Sens. Environ.* **2016**, *173*, 224–237. [CrossRef]
5. Watson, D.J. Comparative physiological studies on the growth of field crops: I. Variation in net assimilation rate and leaf area between species and varieties, and within and between years. *Ann. Bot.* **1947**, *11*, 41–76. [CrossRef]
6. Chen, J.M.; Black, T.A. Defining leaf area index for non-flat leaves. *Plant Cell Environ.* **1992**, *15*, 421–429. [CrossRef]
7. Woodgate, W.; Disney, M.; Armston, J.D.; Jones, S.D.; Suarez, L.; Hill, M.J.; Mellor, A. An improved theoretical model of canopy gap probability for leaf area index estimation in woody ecosystems. *For. Ecol. Manag.* **2015**, *358*, 303–320. [CrossRef]
8. Finney, M.A. *FARSITE: Fire Area Simulator: Model Development and Evaluation*; US Department of Agriculture, Forest Service, Rocky Mountain Research Station: Ogden, UT, USA, 2004.
9. Morsdorf, F.; Kötz, B.; Meier, E.; Itten, K.I.; Allgöwer, B. Estimation of LAI and fractional cover from small footprint airborne laser scanning data based on gap fraction. *Remote Sens. Environ.* **2006**, *104*, 50–61. [CrossRef]
10. Kwak, D.A.; Lee, W.K.; Cho, H.K. Estimation of LAI using LiDAR remote sensing in forest. In Proceedings of the ISPRS Workshop on Laser Scanning 2007 and SilviLaser 2007, Espoo, Finland, 12–14 September 2007.
11. Nelson, R.; Krabill, W.; Tonelli, J. Estimating forest biomass and volume using airborne laser data. *Remote Sens. Environ.* **1988**, *24*, 247–267. [CrossRef]
12. Lefsky, M.A.; Cohen, W.B.; Parker, G.G.; Harding, D.J. LiDAR remote sensing for ecosystem studies. *Bioscience* **2002**, *52*, 19–30. [CrossRef]
13. Solberg, S. Comparing discrete echoes counts and intensity sums from ALS for estimating forest LAI and gap fraction. In Proceedings of the SilviLaser 2008: 8th International Conference on LiDAR Applications in Forest Assessment and Inventory, Edinburgh, UK, 17–19 September 2008.
14. Peduzzi, A.; Wynne, R.H.; Fox, T.R.; Nelson, R.F.; Thomas, V.A. Estimating leaf area index in intensively managed pine plantations using airborne laser scanner data. *For. Ecol. Manag.* **2012**, *270*, 54–65. [CrossRef]
15. Coren, F.; Sterzai, P. Radiometric correction in laser scanning. *Int. J. Remote Sens.* **2006**, *27*, 3097–3104. [CrossRef]
16. Qin, Y.; Yao, W.; Vu, T.T.; Li, S.; Niu, Z.; Ban, Y. Characterizing radiometric attributes of point cloud using a normalized reflective factor derived from small footprint LiDAR waveform. *IEEE J. Sel. Top. Appl. Earth Obs. Remote Sens.* **2015**, *8*, 740–749. [CrossRef]
17. Fang, W.; Huang, X.; Zhang, F.; Li, D. Intensity correction of terrestrial laser scanning data by estimating laser transmission function. *IEEE Trans. Geosci. Remote Sens.* **2015**, *53*, 942–951. [CrossRef]
18. Carrea, D.; Abellan, A.; Humair, F.; Matasci, B.; Derron, M.H.; Jaboyedoff, M. Correction of terrestrial LiDAR intensity channel using Oren–Nayar reflectance model: An application to lithological differentiation. *ISPRS J. Photogramm. Remote Sens.* **2016**, *113*, 17–29. [CrossRef]
19. Tan, K.; Cheng, X.; Ding, X.; Zhang, Q. Intensity data correction for the distance effect in terrestrial laser scanners. *IEEE J. Sel. Top. Appl. Earth Obs. Remote Sens.* **2016**, *9*, 304–312. [CrossRef]
20. Kaasalainen, S.; Ahokas, E.; Hyyppa, J.; Suomalainen, J. Study of surface brightness from backscattered laser intensity: Calibration of laser data. *IEEE Geosci. Remote Sens.* **2005**, *2*, 255–259. [CrossRef]

21. Kaasalainen, S.; Hyyppä, J.; Litkey, P.; Hyyppä, H.; Ahokas, E.; Kukko, A.; Kaartinen, H. Radiometric calibration of ALS intensity. *Int. Arch. Photogramm. Remote Sens.* **2007**, *36*, 201–205.
22. Gross, H.; Jutzi, B.; Thoennessen, U. Intensity normalization by incidence angle and range of full-waveform LiDAR data. *Int. Arch. Photogramm. Remote Sens. Spat. Inf. Sci.* **2008**, *37*, 405–412.
23. Wagner, W. Radiometric calibration of small-footprint full-waveform airborne laser scanner measurements: Basic physical concepts. *ISPRS J. Photogramm. Remote Sens.* **2010**, *65*, 505–513. [CrossRef]
24. Mesas-Carrascosa, F.J.; Castillejo-González, I.L.; de la Orden, M.S.; Porras, A.G.F. Combining LiDAR intensity with aerial camera data to discriminate agricultural land uses. *Comput. Electron. Agric.* **2012**, *84*, 36–46. [CrossRef]
25. Yan, W.Y.; Shaker, A.; Habib, A.; Kersting, A.P. Improving classification accuracy of airborne LiDAR intensity data by geometric calibration and radiometric correction. *ISPRS J. Photogramm. Remote Sens.* **2012**, *67*, 35–44. [CrossRef]
26. Korpela, I.; Ørka, H.O.; Hyyppä, J.; Heikkinen, V.; Tokola, T. Range and AGC normalization in airborne discrete-return LiDAR intensity data for forest canopies. *ISPRS J. Photogramm. Remote Sens.* **2010**, *65*, 369–379. [CrossRef]
27. Höfle, B.; Pfeifer, N. Correction of laser scanning intensity data: Data and model-driven approaches. *ISPRS J. Photogramm. Remote Sens.* **2007**, *62*, 415–433. [CrossRef]
28. Wagner, W.; Hollaus, M.; Briese, C.; Ducic, V. 3D vegetation mapping using small-footprint full-waveform airborne laser scanners. *Int. J. Remote Sens.* **2008**, *29*, 1433–1452. [CrossRef]
29. Hopkinson, C.; Chasmer, L. Testing LiDAR models of fractional cover across multiple forest ecozones. *Remote Sens. Environ.* **2009**, *113*, 275–288. [CrossRef]
30. Heiskanen, J.; Korhonen, L.; Hietanen, J.; Pellikka, P.K. Use of airborne LiDAR for estimating canopy gap fraction and leaf area index of tropical montane forests. *Int. J. Remote Sens.* **2015**, *36*, 2569–2583. [CrossRef]
31. Solberg, S. Mapping gap fraction, LAI and defoliation using various ALS penetration variables. *Int. J. Remote Sens.* **2010**, *31*, 1227–1244. [CrossRef]
32. Luo, S.Z.; Wang, C.; Zhang, G.B.; Xi, X.H.; Li, G.C. Forest leaf area index (LAI) estimation using airborne discrete-return LiDAR data. *Chin. J. Geophys.* **2013**, *56*, 233–242.
33. Solberg, S.; Brunner, A.; Hanssen, K.H.; Lange, H.; Næsset, E.; Rautiainen, M.; Stenberg, P. Mapping LAI in a Norway spruce forest using airborne laser scanning. *Remote Sens. Environ.* **2009**, *113*, 2317–2327. [CrossRef]
34. Sumnall, M.J.; Fox, T.R.; Wynne, R.H.; Blinn, C.; Thomas, V.A. Estimating leaf area index at multiple heights within the understorey component of Loblolly pine forests from airborne discrete-return LiDAR. *Int. J. Remote Sens.* **2016**, *37*, 78–99. [CrossRef]
35. Van Gardingen, P.; Jackson, G.; Hernandez-Daumas, S.; Russell, G.; Sharp, L. Leaf area index estimates obtained for clumped canopies using hemispherical photography. *Agric. For. Meteorol.* **1999**, *94*, 243–257. [CrossRef]
36. Zhao, K.; Popescu, S. Lidar-based mapping of leaf area index and its use for validating GLOBCARBON satellite LAI product in a temperate forest of the southern USA. *Remote Sens. Environ.* **2009**, *113*, 1628–1645. [CrossRef]
37. Schaefer, M.; Farmer, E.; Soto-Berelov, M.; Woodgate, W.; Jones, S. Overview of Ground Based Techniques for Estimating LAI. In *AusCover Good Practice Guidelines: A Technical Handbook Supporting Calibration and Validation Activities of Remotely Sensed Data Product*; TERN AusCover: Canberra, Australia, 2015.
38. Alonzo, M.; Bookhagen, B.; McFadden, J.P.; Sun, A.; Roberts, D.A. Mapping urban forest leaf area index with airborne LiDAR using penetration metrics and allometry. *Remote Sens. Environ.* **2015**, *162*, 141–153. [CrossRef]
39. Kötz, B.; Schaepman, M.; Morsdorf, F.; Bowyer, P.; Itten, K.; Allgöwer, B. Radiative transfer modeling within a heterogeneous canopy for estimation of forest fire fuel properties. *Remote Sens. Environ.* **2004**, *92*, 332–344. [CrossRef]
40. Zhang, K.; Chen, S.C.; Whitman, D.; Shyu, M.L.; Yan, J.; Zhang, C. A progressive morphological filter for removing nonground measurements from airborne LiDAR data. *IEEE Trans. Geosci. Remote Sens.* **2003**, *41*, 872–882. [CrossRef]
41. Axelsson, P. DEM generation from laser scanner data using adaptive TIN models. *Int. Arch. Photogramm. Remote Sens.* **2000**, *33*, 111–118.

42. Sumnall, M.; Peduzzi, A.; Fox, T.R.; Wynne, R.H.; Thomas, V.A.; Cook, B. Assessing the transferability of statistical predictive models for leaf area index between two airborne discrete return LiDAR sensors designs within multiple intensely managed loblolly pine forest locations in the south-eastern USA. *Remote Sens. Environ.* **2016**, *176*, 308–319. [CrossRef]
43. Jelalian, A.V. Laser radar systems. In Proceedings of the Electronics and Aerospace Systems Conference, Arlington, VA, USA, 29 September–1 October 1980.
44. Jutzi, B.; Stilla, U. Range determination with waveform recording laser systems using a wiener filter. *ISPRS J. Photogramm. Remote Sens.* **2006**, *61*, 95–107. [CrossRef]
45. Roncat, A.; Bergauer, G.; Pfeifer, N. B-spline deconvolution for differential target cross-section determination in full-waveform laser scanning data. *ISPRS J. Photogramm. Remote Sens.* **2011**, *66*, 418–428. [CrossRef]
46. Yan, W.Y.; Shaker, A. Radiometric correction and normalization of airborne LiDAR intensity data for improving land-cover classification. *IEEE Trans. Geosci. Remote Sens.* **2014**, *52*, 7658–7673.
47. García, M.; Riaño, D.; Chuvieco, E.; Danson, F.M. Estimating biomass carbon stocks for a Mediterranean forest in central Spain using LiDAR height and intensity data. *Remote Sens. Environ.* **2010**, *114*, 816–830. [CrossRef]
48. Gatziolis, D. Dynamic range-based intensity normalization for airborne, discrete return LiDAR data of forest canopies. *Photogramm. Eng. Remote Sens.* **2011**, *77*, 251–259. [CrossRef]
49. Shaker, A.; Yan, W.Y.; El-Ashmawy, N. The effects of laser reflection angle on radiometric correction of airborne LiDAR intensity data. In Proceedings of the ISPRS Workshop Laser Scanning, Calgary, AB, Canada, 29–31 August 2011.
50. Rees, G.; Rees, W.G. *Physical Principles of Remote Sensing*; Cambridge University Press: Cambridge, UK, 2013.
51. Kaasalainen, S.; Jaakkola, A.; Kaasalainen, M.; Krooks, A.; Kukko, A. Analysis of incidence angle and distance effects on terrestrial laser scanner intensity: Search for correction methods. *Remote Sens.* **2011**, *3*, 2207–2221. [CrossRef]
52. Lefsky, M.A.; Harding, D.; Cohen, W.; Parker, G.; Shugart, H. Surface LiDAR remote sensing of basal area and biomass in deciduous forests of eastern Maryland, USA. *Remote Sens. Environ.* **1999**, *67*, 83–98. [CrossRef]
53. Jensen, J.L.; Humes, K.S.; Vierling, L.A.; Hudak, A.T. Discrete return LiDAR -based prediction of leaf area index in two conifer forests. *Remote Sens. Environ.* **2008**, *112*, 3947–3957. [CrossRef]
54. Korhonen, L.; Korpela, I.; Heiskanen, J.; Maltamo, M. Airborne discrete-return LiDAR data in the estimation of vertical canopy cover, angular canopy closure and leaf area index. *Remote Sens. Environ.* **2011**, *115*, 1065–1080. [CrossRef]
55. Kayitakire, F.; Hamel, C.; Defourny, P. Retrieving forest structure variables based on image texture analysis and IKONOS-2 imagery. *Remote Sens. Environ.* **2006**, *102*, 390–401. [CrossRef]
56. Hopkinson, C. The influence of flying altitude, beam divergence, and pulse repetition frequency on laser pulse return intensity and canopy frequency distribution. *Can. J. Remote Sens.* **2007**, *33*, 312–324. [CrossRef]
57. Sasaki, T.; Imanishi, J.; Ioki, K.; Song, Y.; Morimoto, Y. Estimation of leaf area index and gap fraction in two broad-leaved forests by using small-footprint airborne LiDAR. *Landsc. Ecol. Eng.* **2016**, *12*, 117–127. [CrossRef]
58. Kukko, A.; Kaasalainen, S.; Litkey, P. Effect of incidence angle on laser scanner intensity and surface data. *Appl. Opt.* **2008**, *47*, 986–992. [CrossRef] [PubMed]
59. Kleman, J. The spectral reflectance of stands of Norway spruce and Scotch pine, measured from a helicopter. *Remote Sens. Environ.* **1986**, *20*, 253–265. [CrossRef]